

Variations of Low-latitude Thermospheric Winds and Temperature during the 2020/2021 Major Sudden Stratospheric Warming as Observed by ICON and GOLD Satellites

Erdal Yiğit¹, Ayden L. S. Gann¹, Alexander S. Medvedev², Federico Gasperini³, Md Nazmus Sakib¹, Qian Wu^{4,5}

¹George Mason University, Department of Physics and Astronomy, Space Weather Lab, Fairfax, VA, USA.

²Max Planck Institute for Solar System Research, Göttingen, Germany.

³Orion Space Solutions, Louisville, CO, USA

⁴High Altitude Observatory, NCAR, Boulder, CO, USA

⁵COSMIC Program UCAR/UCP, Boulder, CO, USA

Key Points:

- Effects of the 2020/2021 SSW on thermospheric winds and temperature are studied using ICON and GOLD satellites
- Thermospheric mean winds undergo substantial changes during the SSW, some changes occurring before the warming onset.
- The low-latitude thermosphere cools around 150 km during the SSW, with a cooling trend starting before the warming onset.

Abstract

Using ICON and GOLD satellite observations, the response of the thermospheric day-time horizontal winds and neutral temperature to the 2020/2021 major sudden stratospheric warming (SSW) is studied at low- to middle latitudes (0° - 40°N). Comparison with observations during the non-SSW winter of 2019/2020 and the pre-SSW period (December 2020) clearly demonstrates the SSW-induced changes. The northward and westward thermospheric winds are enhanced during the warming event, while temperature around 150 km drops by up to about 50 K compared to the pre-SSW phase. Changes in the horizontal circulation during the SSW can generate upwelling at low-latitudes, which can contribute to the adiabatic cooling of the low-latitude thermosphere. The observed changes during the major SSW are a manifestation of long-range vertical coupling in the atmosphere.

Plain Language Summary

NASA's ICON and GOLD satellites are used to determine to what extent the 2020/2021 major sudden stratospheric warming (SSW) influenced the thermosphere above 90 km. Observations show that the horizontal circulation becomes more westward and poleward and the temperature cools by up to 50 K during the warming event. Changes in the stratospheric circulation during the major SSW modulate the upward propagation of atmospheric waves of various scales. These altered waves can reach the thermosphere, interact with the background atmosphere and induce upward motions at low-latitudes, thus explaining, to some degree, the significant cooling observed by GOLD. Our observations provide evidence for SSW-induced long-range vertical coupling in the atmosphere.

1 Introduction

Sudden stratospheric warmings (SSWs) are remarkable phenomena that occur in the polar lower stratosphere (mostly in the Northern hemisphere) during winters and last for several days. Although five types of warmings are currently distinguished – major, midwinter, minor, final, and Canadian (Butler et al., 2015), – they often are categorized as either major or minor events. In a major warming, the zonal mean winds \bar{u} at 60°N reverse their direction from eastward to westward at or below 10 hPa (~ 30 km) and the zonal mean temperature \bar{T} increases poleward of 60°N . During a minor warming, the zonal mean temperature increases poleward of 60°N , while the eastward zonal mean winds weaken but do not fully reverse. SSWs are caused by large-scale planetary waves propagating upward from the troposphere and interacting with the stratospheric mean flow (Holton, 1976; Matsuno, 1971).

The dynamical and thermodynamical effects of SSWs are wide-reaching and include not only the troposphere-stratosphere coupling, but extend across all layers from the troposphere to the thermosphere and ionosphere (Yiğit & Medvedev, 2015; Miyoshi et al., 2015; Goncharenko et al., 2021). While the peak of temperature increase occurs over the pole (usually at North), these events produce changes across the hemisphere that last for several weeks. The lower and middle atmospheric effects of SSWs have been extensively studied (Siskind et al., 2010; Gu et al., 2020; Roy & Kuttippurath, 2022), however the response of the upper atmosphere to SSWs is understood to a lesser degree. Nevertheless, an increasing amount of modeling efforts and observations provided a solid framework for characterizing the SSW effects in the upper atmosphere (Goncharenko et al., 2021; Koucká Knížová et al., 2021).

A variety of observational and modeling techniques have been used to quantify the response of the thermosphere-ionosphere to SSWs. Sudden warmings affect both the mean state and variability of thermospheric temperatures and horizontal winds at various scales, as simulated by general circulation models (GCMs) (Miyoshi et al., 2015; Liu et al., 2013).

Observations demonstrated a persistent connection between the 2009 major SSW and the ionospheric variations at low-latitudes (Goncharenko, Chau, et al., 2010). They revealed that the SSW-induced changes in the ionosphere increase the latitudinal asymmetry of the equatorial ionization anomaly (Azeem et al., 2015). Studies of ionospheric variations with ground-based measurements by digisondes at midlatitudes showed that the peak electron density around the F₂ region and TEC increased during an SSW (Mošna et al., 2021).

Gravity (buoyancy) waves (GW) and solar tides of various scales propagate directly from the lower atmosphere to the thermosphere producing multi-scale coupling and influence the general circulation and temperature structure of the upper atmosphere (Yiğit & Medvedev, 2009; Miyoshi & Fujiwara, 2008; Heale et al., 2014; Gavrilov & Kshevetskii, 2015; Gasperini et al., 2022; Pancheva et al., 2009). SSWs alter the propagation and dissipation of atmospheric waves in the whole atmosphere system (Yiğit & Medvedev, 2016). While during minor warmings GW activity increases in the thermosphere (Yiğit & Medvedev, 2012; Yiğit et al., 2014), during a major warming, GW activity in the ionosphere can slightly increase in the early phase, but ultimately decreases in the main phase of the warming, as demonstrated by GPS-TEC analysis (Nayak & Yiğit, 2019). Also, high resolution GCMs show that the total GW energy and the associated drag decrease in the thermosphere above 110 km (Miyoshi et al., 2015), while observations show that nonmigrating tides amplify in the middle atmosphere (Pancheva et al., 2009). More recently, analysis of the ICON observations between 93–106 km indicated that the semidiurnal tidal and 3-day ultra-fast Kelvin wave activity contribute to the structure of the mean meridional circulation in the upper mesosphere and lower thermosphere (MLT) (Gasperini et al., 2023).

Planetary wave amplification with subsequent breaking and changes in GW dynamics can significantly modify the stratospheric and mesospheric circulation and temperature during major SSWs (Siskind et al., 2010, 2005; Gavrilov et al., 2018; Gu et al., 2020; Koval et al., 2021). The impact of SSWs on the thermospheric winds, circulation, and temperature has been insufficiently explored, due primarily to limited coverage in observations. In this paper, we use ICON and GOLD horizontal wind and temperature measurements for characterizing the impact of the major 2020/2021 SSW on the low-latitude thermosphere. This is the first observational study that reports on coincident measurements of wind and temperature above 120 km during the major warming event, which commenced on 1st January 2021, peaked on 5th January 2021 and lasted for a few weeks.

2 Observations and Data Analysis

We employ the measurements of horizontal winds by ICON (Immel et al., 2018) and of temperature by GOLD satellites (Eastes et al., 2017). Specifically, we consider the ICON/MIGHTI version 5 zonal and meridional winds based on green line measurements along with the GOLD neutral temperatures obtained from Level 2 (L2) T_{disk} version 4 data. ICON observes the thermosphere at low- to midlatitudes ($\sim 10^\circ\text{S}$ - 40°N). Characterization of the mean horizontal winds and the associated circulation by ICON/MIGHTI for the Northern Hemisphere summer solstice has recently been performed in the work by Yiğit et al. (2022). GOLD measures the Far Ultraviolet (FUV) spectrum of Earth's atmosphere at geostationary orbit, from 0610 to 0040 Universal Time (UT) every day, providing, among others, daytime thermospheric temperatures near 150 km at low- and midlatitudes (0° to $\pm 60^\circ$), depending on the solar zenith angle (see Section 1 in SI for further information).

We first characterize the SSW in the stratosphere based on the MERRA-2 reanalysis data output every three hours and compare with a non-SSW winter. **Figure 1** shows the evolution of the December 2020–January 2021 major SSW at 10 hPa (30 km) in terms of the zonal mean temperature \bar{T} and zonal wind \bar{u} (red lines). They are compared with

those for the non-SSW winter of December 2019–January 2020 (black lines). The temperature is plotted at 60°N and 90°N and the zonal wind at 35°N and 60°N. **Figure 1** demonstrates that, after the onset of the warming on 1 January 2021, the Northern polar temperature increases by 50 K – from about 200 K to 250 K, peaking on 5 January 2021. During the ascending phase of the warming, \bar{u} at 60°N gradually changes to westward – from $\sim 30 \text{ m s}^{-1}$ at the onset of the SSW to about -10 m s^{-1} at the peak phase, demonstrating a reversal of the mean flow direction. The recovery phase of the SSW is relatively long, during which the temperatures remain elevated and \bar{u} is westward compared to the pre-SSW period in December 2020 and during the non-SSW season in January 2021. It is noticeable that the December 2019 (non-SSW winter) and December 2020 exhibit some minor differences in mean winds, owing, partially, to interannual variations in planetary wave activity and behavior of large-scale internal waves.

For the thermospheric data from both instruments, we selected a period centered around the onset of the SSW, i.e., from 6 December 2020 to 26 January 2021 (hereafter called “SSW winter”). The results are compared to those for the non-SSW winter (6 December 2019 to 26 January 2020). While between ~ 90 – 109 km both daytime and nighttime data are available, only daytime winds are available above $\sim 109 \text{ km}$ up to about 210 km . Therefore, we use only daytime winds from 90 – 200 km to produce a uniform analysis of the mean wind variations.

The solar and geomagnetic activity were relatively low during the studied periods, with somewhat higher solar activity during the SSW winter ($F_{10.7} \sim 75$ – $90 \text{ W m}^{-2} \text{ Hz}^{-1}$ vs $F_{10.7} \sim 70$ – $75 \text{ W m}^{-2} \text{ Hz}^{-1}$ for the non-SSW period). The magnetic activity, although generally low, exhibits some degree of day-to-day variability, reaching occasionally $A_p \sim 12$ ($K_p \sim 3$) (see Section 2 and Figure S3 in Supporting Information for details). In order to reduce the impact of these elevated space weather conditions on our analysis of temperature variations, we have excluded geomagnetically disturbed days with $A_p > 7$ ($K_p > 2$) in temperature plots.

3 Results and Discussion

3.1 Observations of Thermospheric Horizontal Winds

In order to assess changes in the thermospheric winds induced by the major SSW, we consider ICON/MIGHTI measurements for two periods with a common spatiotemporal coverage. **Figure 2** presents the evolution of the daytime zonal mean horizontal winds during the SSW (December 2020 – January 2021) and non-SSW winters (December 2019 – January 2020) at two representative latitude bands: at low-latitude (0 – 20°N) and low- to midlatitude (20° – 40°N) regions. Altitudes and days, for which observations are not available, are shown in gray shading.

Even without an SSW, the observed thermospheric horizontal winds exhibit a significant degree of day-to-day variability. This could be related to a combination of physical processes, such as a) changes in the dynamics of internal atmospheric waves, b) variability of the solar and geomagnetic activity, and c) orbital effects, e.g., ICON’s orbit precession toward earlier local times by about 29.8 min every day (see Figure S1 and Section 1 in Supporting Information). Under the non-SSW conditions (during the non-SSW winter and before the onset of the warming), the daytime mean zonal winds exhibit an alternating with altitude pattern at low- and low- to midlatitudes: typically eastward in the upper mesosphere, westward in the lower thermosphere and eastward again above $\sim 140 \text{ km}$. Above $\sim 160 \text{ km}$, the westward flow dominates, in general. The mean daytime meridional winds without an SSW are overall northward (representing the summer-to-winter circulation) in the upper mesosphere, southward (winter-to-summer transport) in the lower thermosphere, and poleward again above $\sim 130 \text{ km}$ (**Figure 2c,g**).

Predominantly westward GWs surviving the winter eastward stratomesospheric jets are responsible for shaping the circulation in the MLT (Yiğit et al., 2009). The associated westward GW momentum deposition reverses the meridional winds in the winter MLT, thereby also reversing the mean zonal winds from eastward to westward (Lilienthal et al., 2020; Yiğit et al., 2021, 2022). The measured wind reversals provide an indirect observational evidence for the momentum transport carried by upward propagating internal waves, in the absence of which, the MLT would remain in radiative balance (Andrews et al., 1987) and the eastward and summer-to-winter meridional flow would dominate in the Northern Hemisphere. The momentum forcing is also supplemented by upward propagating diurnal and semidiurnal tides at low- and middle-latitudes, respectively (Griffith et al., 2021; Miyoshi & Yiğit, 2019; Jones et al., 2019).

After the onset of the warming in January 2021 (Figures 2b,d,f,h), westward (negative) and northward (positive) winds relatively strengthen depending on the altitude and day, especially above 140 km. There is an indication that the thermospheric winds begin to change before the start of the SSW, which can probably be related to the fact that the stratospheric mean zonal wind decrease precedes the polar temperature rise by several days (Figure 1b). This phenomenon is known to modulate upward gravity wave propagation (Yiğit & Medvedev, 2012; Miyoshi et al., 2015).

3.2 Observations of Thermospheric Temperature

Figure 3 presents the day-to-day evolution of the daytime neutral temperatures near 150 km measured by GOLD and averaged zonally and over the same two representative latitude bands discussed above. Based on GOLD's coverage, only longitudes between 100°W and 10°E contributed to the zonal mean. The upper two rows (Figures 3a,b,c,d) show the temperature variations as a function of solar zenith angle χ . Note that the two latitude bands have different χ coverage. The observations for $25^\circ < \chi < 65^\circ$ contributed to the low-latitude 0 - 20°N band, with a larger portion of measurements centered around 65°. The low- to midlatitude (20° - 40°N) band includes observations for χ between 45° and 65°, with a larger portion taken around $\chi = 55^\circ$. Rows three and four (Figures 3e,f) display another aspect of temperature variations: the latitude-time cross-sections at 150 km during the non-SSW and SSW winters, respectively. It is seen that, at all latitudes and solar zenith angles, thermospheric temperatures drop during the SSW. The cooling trend begins shortly before the SSW onset and lasts for about 15 days. The thermospheric cooling is more clearly seen in **Figure 4**, which presents the day-to-day variations of the average temperature in the corresponding latitude bands. The error bars indicate the variability around a fitted linear trend (see Section 1 in SI for further information). Starting a few days before the onset of the SSW, the thermospheric temperature decreases by about 50 K, from ~ 730 K to 680 K, after which it returns back to ~ 720 K over about ten days. Such cooling trend is untypical in the low-latitude thermosphere in the absence of SSWs, as a comparison with the non-SSW winter shows. It is also seen that the thermosphere is much colder during the non-SSW winter, because it coincided with the solar minimum.

3.3 Possible Mechanisms of Thermal Changes and Connections to Winds in the Low-Latitude Thermosphere

Observations presented above demonstrate a global response of the low- to middle-latitude thermosphere to the SSW event. Generally, winds and neutral temperature are affected by a number of physical processes pertaining to external (space weather, or coupling from above) and internal forcing (coupling from below) (Yiğit et al., 2016). Originated in the troposphere and lower stratosphere, SSWs represent remarkable disturbances of the latter type, which rapidly disrupt vertical propagation of atmospheric waves that can directly propagate to thermospheric altitudes. A number of observational and modeling studies found that the thermospheric GW activity decreases after a major warm-

ing is fully developed (Nayak & Yiğit, 2019; Miyoshi et al., 2015). On the other hand, the amplitude of the migrating Sun-synchronous semidiurnal tide increases during SSWs in the low- and midlatitude lower and upper thermosphere (Goncharenko, Coster, et al., 2010; Liu et al., 2013; Oberheide, 2022). These two changes can be related, because GWs are known to attenuate the semidiurnal tide in the thermosphere (Miyoshi & Yiğit, 2019). Semidiurnal tidal sources can also be modulated owing to a redistribution of the stratospheric ozone. Thus, the modified wave forcing can directly affect the residual circulation in the thermosphere (Koval et al., 2021). Systematic modeling studies are required for isolating the effects of gravity waves and semidiurnal tides (and their possible interactions) during stratospheric warmings.

SSW-induced thermal and dynamical changes are intimately connected. In addition to direct wave forcing, they can be caused by modification of the large-scale flow. Divergence and convergence of horizontal winds are a source of vertical motions (Rishbeth et al., 1969) and of the associated adiabatic heating/cooling. Using simulations with a whole atmosphere model, Liu et al. (2013) reported a net cooling of the thermosphere above 100 km during the 2008/2009 major SSW, which is qualitatively in agreement with our observations. A net upwelling and enhanced poleward flow initiated by SSW-induced changes can account for the observed cooling in the low-latitude thermosphere around 150 km.

Finally, a subtle decrease of solar activity (from 85 to $75 \times 10^{-22} \text{ W m}^{-2} \text{ s}^{-1}$) over the SSW period (see Figure S3) can contribute to some extent to the observed 50 K temperature drop around 150 km. Tests with the NRLMSIS empirical model (Picone et al., 2002) suggest that a reduction of the solar activity by 10 $F_{10.7}$ radio flux units changes temperature by only 5–10 K around 150 km altitude (not shown). Obviously, more accurate and self-consistent estimates can be obtained using whole atmosphere general circulation modeling.

4 Summary & Conclusions

Combining ICON and GOLD satellite observations, we have explored the impact of the 2020/2021 major sudden stratospheric warming (SSW) on the thermospheric horizontal circulation between 90 and 200 km and temperatures around 150 km. Wind and temperature variations during the SSW have been compared to the pre- and non-SSW periods. The main inferences of our study are as follows:

1. Horizontal winds exhibit a significant degree of day-to-day variability during all times, which are related to a combination of orbital changes (e.g., day-to-day change in local time coverage) and physical and dynamical processes.
2. Low- to midlatitude zonal winds are typically eastward in the upper mesosphere; reverse their direction to westward in the lower thermosphere, and change again to eastward above ~ 120 km. Above ~ 160 km, the westward flow dominates, in general. Mean daytime meridional winds are overall northward (poleward, representing the summer-to-winter transport) in the upper mesosphere, southward (equatorward, or winter-to-summer flow) in the lower thermosphere, and poleward again above ~ 130 km.
3. After the onset of the warming, westward and northward winds strengthen depending on the altitude and day, especially above 140 km. There is an indication that the thermospheric winds begin to change before the start of the SSW.
4. The low-latitude thermosphere cools down during the SSW by about 50 K. The cooling trend starts about 7–10 days before the onset of the warming in the stratosphere and lasts for about two weeks. The recovery phase of the temperature takes about ten days.

5. SSW-induced thermal and dynamical changes are intimately connected. The observed temperature drop in the thermosphere is likely caused by adiabatic cooling associated with changes in the large-scale horizontal flow.

Data Availability Statement

The MIGHTI horizontal wind data (version 5) used in this study are available at the ICON data center (<https://icon.ssl.berkeley.edu/Data>). The GOLD level 2 data used in this study are available at the GOLD Science Data Center (<https://gold.cs.ucf.edu/search/>) and at NASA's Space Physics Data Facility (<https://spdf.gsfc.nasa.gov/pub/data/gold/level2/tdisk>).

Acknowledgments

This work was supported by NASA (Grant 80NSSC22K0016). FG acknowledges support from NASA GIGI Grant 80NSSC22K0019. ICON is supported by NASA's Explorers Program through contracts NNG12FA45C and NNG12FA42I. MNS was supported by the National Science Foundation under Grant No. 1849014

References

- Andrews, D. G., Taylor, F. W., & McIntyre, M. E. (1987). The influence of atmospheric waves on the general circulation of the middle atmosphere. *Phil. Trans. R. Soc. Lond. A*, *323*(1575), 693–705. doi: 10.1098/rsta.1987.0115
- Azeem, I., Crowley, G., & Honniball, C. (2015). Global ionospheric response to the 2009 sudden stratospheric warming event using Ionospheric Data Assimilation Four-Dimensional (IDA4D) algorithm: Ionosphere during Stratospheric Warming. *J. Geophys. Res. Space Physics*, *120*(5), 4009–4019. doi: 10.1002/2015JA020993
- Butler, A. H., Seidel, D. J., Hardiman, S. C., Butchart, N., Birner, T., & Match, A. (2015). Defining Sudden Stratospheric Warmings. *Bulletin of the American Meteorological Society*, *96*(11), 1913–1928. doi: 10.1175/BAMS-D-13-00173.1
- Eastes, R. W., McClintock, W. E., Burns, A. G., Anderson, D. N., Andersson, L., Codrescu, M., ... Oberheide, J. (2017). The Global-Scale Observations of the Limb and Disk (GOLD) Mission. *Space Sci Rev*, *212*(1), 383–408. doi: 10.1007/s11214-017-0392-2
- Gasperini, F., Crowley, G., Immel, T. J., & Harding, B. J. (2022). Vertical Wave Coupling in the Low-Latitude Ionosphere-Thermosphere as Revealed by Concurrent ICON and COSMIC-2 Observations. *Space Sci Rev*, *218*(7), 55. doi: 10.1007/s11214-022-00923-1
- Gasperini, F., Jones Jr, M., Harding, B. J., & Immel, T. J. (2023). Direct Observational Evidence of Altered Mesosphere Lower Thermosphere Mean Circulation From a Major Sudden Stratospheric Warming. *Geophysical Research Letters*, *50*(7), e2022GL102579. doi: 10.1029/2022GL102579
- Gavrilov, N. M., Koval, A. V., Pogoreltsev, A. I., & Savenkova, E. N. (2018). Simulating planetary wave propagation to the upper atmosphere during stratospheric warming events at different mountain wave scenarios. *Advances in Space Research*, *61*(7), 1819–1836. doi: 10.1016/j.asr.2017.08.022
- Gavrilov, N. M., & Kshevetskii, S. P. (2015). Dynamical and thermal effects of non-steady nonlinear acoustic-gravity waves propagating from tropospheric sources to the upper atmosphere. *Advances in Space Research*, *56*(9), 1833–1843. doi: 10.1016/j.asr.2015.01.033
- Goncharenko, L. P., Chau, J. L., Liu, H.-L., & Coster, A. J. (2010). Unexpected connections between the stratosphere and ionosphere. *Geophys. Res. Lett.*, *37*(10), n/a-n/a. doi: 10.1029/2010GL043125

- 318 Goncharenko, L. P., Coster, A. J., Chau, J. L., & Valladares, C. E. (2010). Im-
 319 pact of sudden stratospheric warmings on equatorial ionization anomaly. *J.*
 320 *Geophys. Res.*, *115*(A10), n/a-n/a. doi: 10.1029/2010JA015400
- 321 Goncharenko, L. P., Harvey, V. L., Liu, H., & Pedatella, N. M. (2021). Sudden
 322 Stratospheric Warming Impacts on the Ionosphere–Thermosphere System. In
 323 *Ionosphere Dynamics and Applications* (pp. 369–400). American Geophysical
 324 Union (AGU). doi: 10.1002/9781119815617.ch16
- 325 Griffith, M. J., Dempsey, S. M., Jackson, D. R., Moffat-Griffin, T., & Mitchell, N. J.
 326 (2021). Winds and tides of the Extended Unified Model in the mesosphere
 327 and lower thermosphere validated with meteor radar observations. *Annales*
 328 *Geophysicae*, *39*(3), 487–514. doi: 10.5194/angeo-39-487-2021
- 329 Gu, S., Hou, X., Qi, J., TengChen, K., Dou, X., & School of Electronic Information,
 330 Wuhan University, Wuhan 430072, China. (2020). Responses of middle atmo-
 331 spheric circulation to the 2009 major sudden stratospheric warming. *Earth and*
 332 *Planetary Physics*, *4*(4), 1–7. doi: 10.26464/epp2020046
- 333 Heale, C. J., Snively, J. B., Hickey, M. P., & Ali, C. J. (2014). Thermospheric dis-
 334 sipation of upward propagating gravity wave packets. *Journal of Geophysical*
 335 *Research*, *16*.
- 336 Holton, J. R. (1976). A semi-spectral numerical model for wave-Mean Flow
 337 Interactions in the Stratosphere: Application to Sudden Stratospheric
 338 Warmings. *Journal of the Atmospheric Sciences*, *33*(8), 1639–1649. doi:
 339 10.1175/1520-0469(1976)033<1639:ASSNMF>2.0.CO;2
- 340 Immel, T. J., England, S. L., Mende, S. B., Heelis, R. A., Englert, C. R., Edel-
 341 stein, J., ... Sirk, M. M. (2018). The Ionospheric Connection Explorer
 342 Mission: Mission Goals and Design. *Space Sci Rev*, *214*(1), 13. doi:
 343 10.1007/s11214-017-0449-2
- 344 Jones, M., Forbes, J. M., & Sassi, F. (2019). The Effects of Vertically Propagating
 345 Tides on the Mean Dynamical Structure of the Lower Thermosphere. *J. Geo-*
 346 *phys. Res. Space Physics*, *124*(8), 7202–7219. doi: 10.1029/2019JA026934
- 347 Koucká Knížová, P., Laštovička, J., Kouba, D., Mošna, Z., Podolská, K.,
 348 Potužníková, K., ... Rusz, J. (2021). Ionosphere Influenced From
 349 Lower-Lying Atmospheric Regions. *Front. Astron. Space Sci.*, *8*. doi:
 350 10.3389/fspas.2021.651445
- 351 Koval, A. V., Chen, W., Didenko, K. A., Ermakova, T. S., Gavrilov, N. M.,
 352 Pogoreltsev, A. I., ... Zarubin, A. S. (2021). Modelling the residual
 353 mean meridional circulation at different stages of sudden stratospheric
 354 warming events. *Annales Geophysicae*, *39*(2), 357–368. doi: 10.5194/
 355 angeo-39-357-2021
- 356 Lilienthal, F., Yiğit, E., Samtleben, N., & Jacobi, C. (2020). Variability of Gravity
 357 Wave Effects on the Zonal Mean Circulation and Migrating Terdiurnal Tide
 358 as Studied With the Middle and Upper Atmosphere Model (MUAM2019)
 359 Using a Nonlinear Gravity Wave Scheme. *Front. Astron. Space Sci.*, *7*. doi:
 360 10.3389/fspas.2020.588956
- 361 Liu, H., Jin, H., Miyoshi, Y., Fujiwara, H., & Shinagawa, H. (2013). Upper at-
 362 mosphere response to stratosphere sudden warming: Local time and height
 363 dependence simulated by GAIA model. *Geophysical Research Letters*, *40*(3),
 364 635–640. doi: 10.1002/grl.50146
- 365 Matsuno, T. (1971). A Dynamical Model of the Stratospheric Sudden Warm-
 366 ing. *Journal of the Atmospheric Sciences*, *28*(8), 1479–1494. doi: 10.1175/
 367 1520-0469(1971)028<1479:ADMOTS>2.0.CO;2
- 368 Miyoshi, Y., & Fujiwara, H. (2008). Gravity Waves in the Thermosphere Simulated
 369 by a General Circulation Model. *J. Geophys. Res.*, *113*(D1), D01101. doi: 10
 370 .1029/2007JD008874
- 371 Miyoshi, Y., Fujiwara, H., Jin, H., & Shinagawa, H. (2015). Impacts of sudden
 372 stratospheric warming on general circulation of the thermosphere. *J. Geophys.*

- Res. Space Physics*, 120(12), 10,897–10,912. doi: 10.1002/2015JA021894
- Miyoshi, Y., & Yiğit, E. (2019). Impact of gravity wave drag on the thermospheric circulation: Implementation of a nonlinear gravity wave parameterization in a whole-atmosphere model. *Ann. Geophys.*, 37(5), 955–969. doi: 10.5194/angeo-37-955-2019
- Mošna, Z., Edemskiy, I., Laštovička, J., Kozubek, M., Koucká Knížová, P., Kouba, D., & Siddiqui, T. A. (2021). Observation of the Ionosphere in Middle Latitudes during 2009, 2018 and 2018/2019 Sudden Stratospheric Warming Events. *Atmosphere*, 12(5), 602. doi: 10.3390/atmos12050602
- Nayak, C., & Yiğit, E. (2019). Variation of Small-Scale Gravity Wave Activity in the Ionosphere During the Major Sudden Stratospheric Warming Event of 2009. *J. Geophys. Res. Space Physics*, 124(1), 470–488. doi: 10.1029/2018JA026048
- Oberheide, J. (2022). Day-to-Day Variability of the Semidiurnal Tide in the F-Region Ionosphere During the January 2021 SSW From COSMIC-2 and ICON. *Geophysical Research Letters*, 49(17), e2022GL100369. doi: 10.1029/2022GL100369
- Pancheva, D., Mukhtarov, P., & Andonov, B. (2009). Nonmigrating tidal activity related to the sudden stratospheric warming in the Arctic winter of 2003/2004. *Ann. Geophys.*, 27(3), 975–987. doi: 10.5194/angeo-27-975-2009
- Picone, J. M., Hedin, A. E., Drob, D. P., & Aikin, A. C. (2002). NRLMSISE-00 empirical model of the atmosphere: Statistical comparisons and scientific issues. *Journal of Geophysical Research: Space Physics*, 107(A12), SIA 15-1-SIA 15-16. doi: 10.1029/2002JA009430
- Rishbeth, H., Moffett, R., & Bailey, G. (1969). Continuity of air motion in the mid-latitude thermosphere. *Journal of Atmospheric and Terrestrial Physics*, 31(8), 1035–1047. doi: 10.1016/0021-9169(69)90103-2
- Roy, R., & Kuttippurath, J. (2022). The dynamical evolution of Sudden Stratospheric Warmings of the Arctic winters in the past decade 2011–2021. *SN Appl. Sci.*, 4(4), 105. doi: 10.1007/s42452-022-04983-4
- Siskind, D. E., Coy, L., & Espy, P. (2005). Observations of stratospheric warmings and mesospheric coolings by the TIMED SABER instrument. *Geophys. Res. Lett.*, 4. doi: 10.1029/2005GL022399
- Siskind, D. E., Eckermann, S. D., McCormack, J. P., Coy, L., Hoppel, K. W., & Baker, N. L. (2010). Case studies of the mesospheric response to recent minor, major, and extended stratospheric warmings. *J. Geophys. Res.*, 115, D00N03. doi: 10.1029/2010JD014114
- Yiğit, E., Dhadly, M., Medvedev, A. S., Harding, B. J., Englert, C. R., Wu, Q., & Immel, T. J. (2022). Characterization of the Thermospheric Mean Winds and Circulation During Solstice Using ICON/MIGHTI Observations. *Journal of Geophysical Research: Space Physics*, 127(11), e2022JA030851. doi: 10.1029/2022JA030851
- Yiğit, E., Koucká Knížová, P., Georgieva, K., & Ward, W. (2016). A review of vertical coupling in the Atmosphere–Ionosphere system: Effects of waves, sudden stratospheric warmings, space weather, and of solar activity. *Journal of Atmospheric and Solar-Terrestrial Physics*, 141, 1–12. doi: 10.1016/j.jastp.2016.02.011
- Yiğit, E., & Medvedev, A. S. (2009). Heating and cooling of the thermosphere by internal gravity waves. *Geophys. Res. Lett.*, 36(14), L14807. doi: 10.1029/2009GL038507
- Yiğit, E., & Medvedev, A. S. (2012). Gravity waves in the thermosphere during a sudden stratospheric warming. *Geophys. Res. Lett.*, 39(21), n/a–n/a. doi: 10.1029/2012GL053812
- Yiğit, E., & Medvedev, A. S. (2015). Internal wave coupling processes in Earth’s atmosphere. *Advances in Space Research*, 55(4), 983–1003. doi: 10.1016/j.asr.2014.11.020

- 428 Yiğit, E., & Medvedev, A. S. (2016). Role of gravity waves in vertical coupling
 429 during sudden stratospheric warmings. *Geosci. Lett.*, *3*(1), 27. doi: 10.1186/
 430 s40562-016-0056-1
- 431 Yiğit, E., Medvedev, A. S., Aylward, A. D., Hartogh, P., & Harris, M. J. (2009).
 432 Modeling the effects of gravity wave momentum deposition on the general
 433 circulation above the turbopause. *J. Geophys. Res.*, *114*(D7), D07101. doi:
 434 10.1029/2008JD011132
- 435 Yiğit, E., Medvedev, A. S., England, S. L., & Immel, T. J. (2014). Simulated vari-
 436 ability of the high-latitude thermosphere induced by small-scale gravity waves
 437 during a sudden stratospheric warming. *Journal of Geophysical Research:*
 438 *Space Physics*, *119*(1), 357–365. doi: 10.1002/2013JA019283
- 439 Yiğit, E., Medvedev, A. S., & Ern, M. (2021). Effects of Latitude-Dependent Grav-
 440 ity Wave Source Variations on the Middle and Upper Atmosphere. *Front. As-*
 441 *tron. Space Sci.*, *7*, 614018. doi: 10.3389/fspas.2020.614018

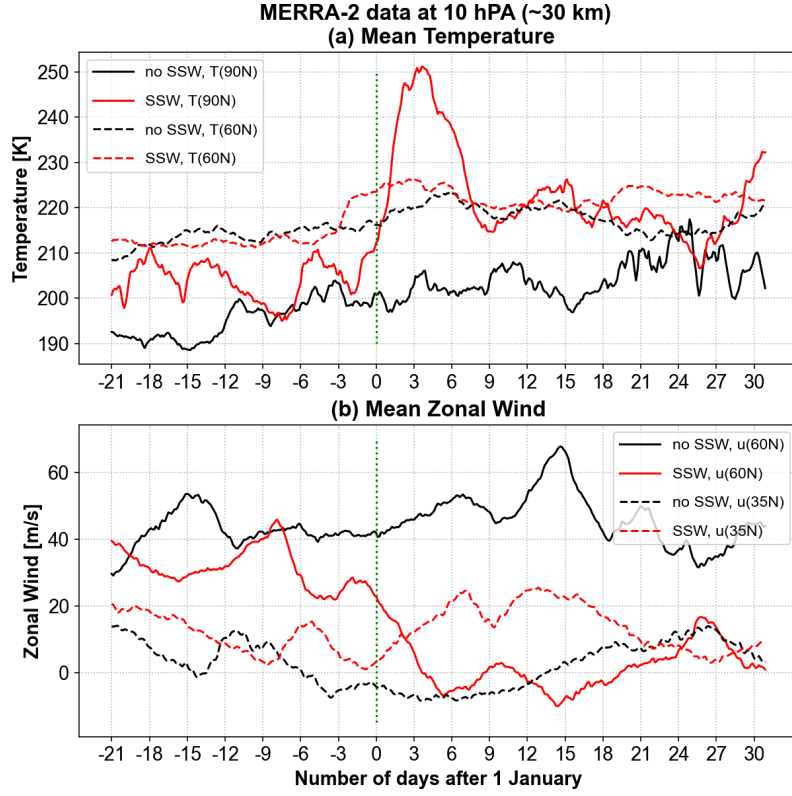
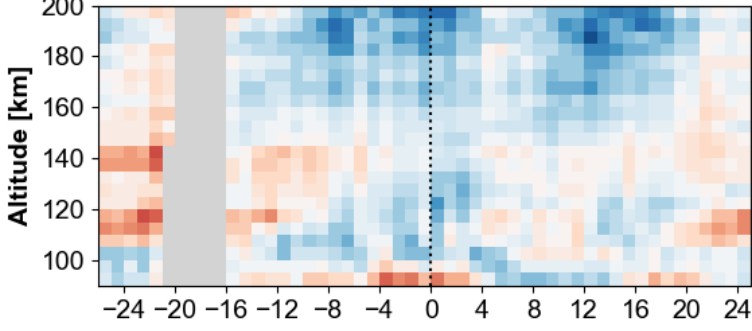
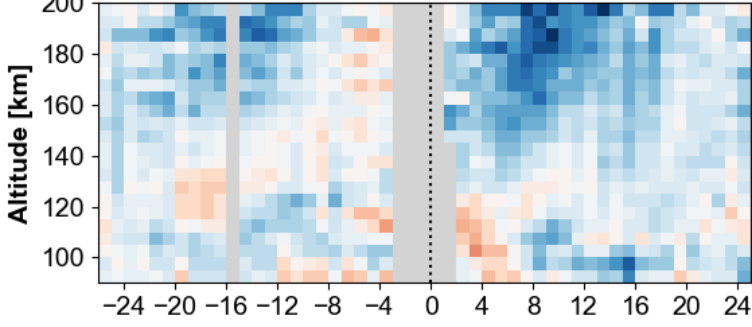
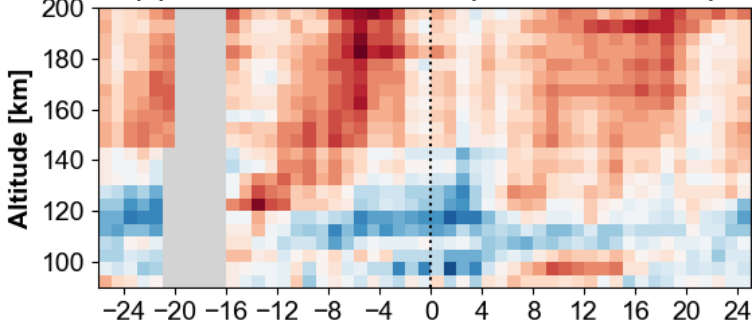
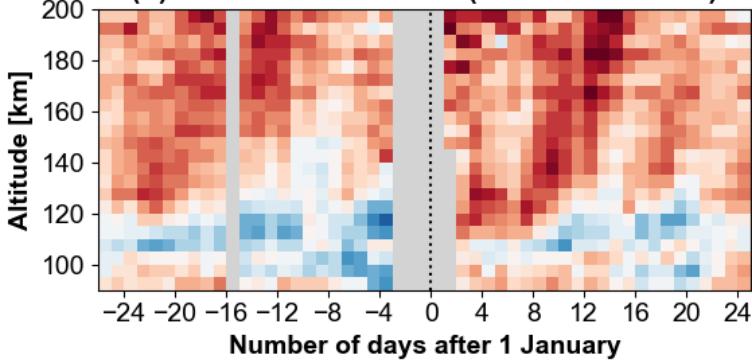


Figure 1. Variation of the zonal mean (a) temperature and (b) zonal winds at 10 hPa (~ 30 km) based on MERRA-2; during the 2019/2020 non-SSW winter (black) and 2020/2021 SSW winter (red). The vertical green dashed lines on the day zero marks the onset of the major warming (i.e. 1 January 2021). Mean temperature is shown at the North Pole and at 60°N ; the mean zonal winds are shown at 35° and 60°N for both winters.

ICON/MIGHTI Daytime Mean Neutral Winds

(0 – 20° N)

(a) Dec 2019 - Jan 2020 (Zonal Wind)**(b) Dec 2020 - Jan 2021 (Zonal Wind)****(c) Dec 2019 - Jan 2020 (Meridional Wind)****(d) Dec 2020 - Jan 2021 (Meridional Wind)**

(20 – 40° N)

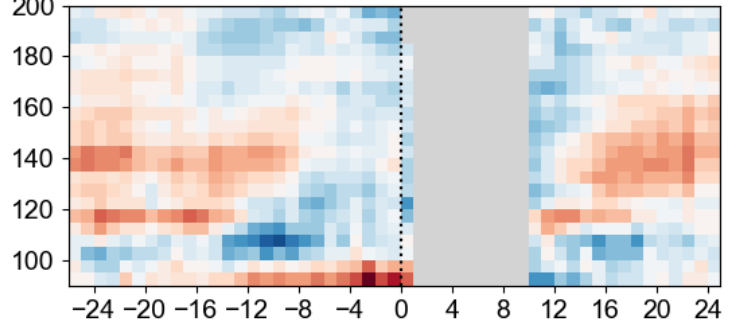
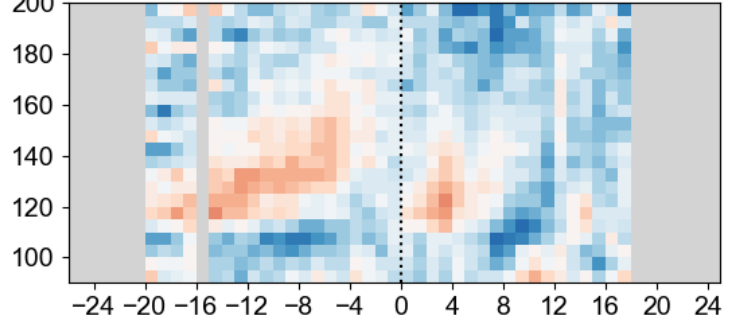
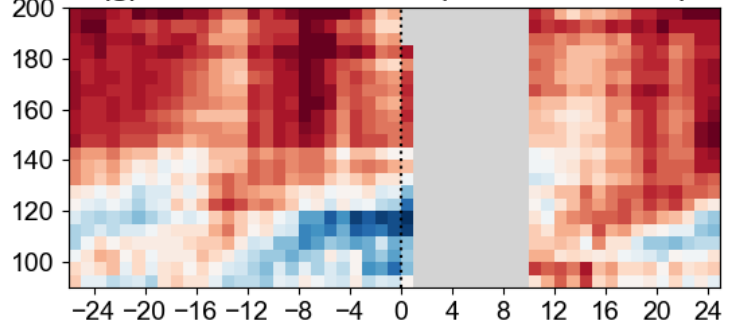
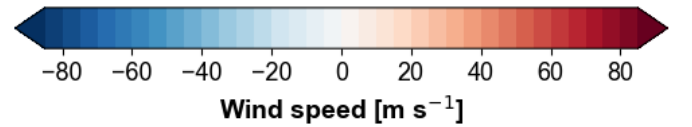
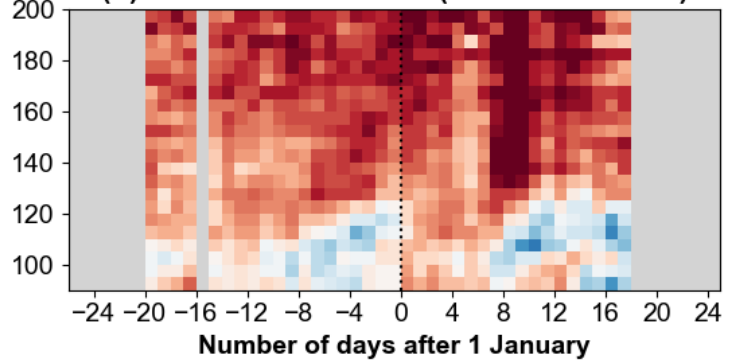
(e) Dec 2019 - Jan 2020 (Zonal Wind)**(f) Dec 2020 - Jan 2021 (Zonal Wind)****(g) Dec 2019 - Jan 2020 (Meridional Wind)****(h) Dec 2020 - Jan 2021 (Meridional Wind)**

Figure 2. Contour plots of the daytime mean zonal winds (upper two rows) and meridional winds (lower two rows) in m/s during the non-SSW winter (December 2019-January 2020, first and third rows) and SSW winter (December 2020-January 2021, second and fourth rows) plotted from 6 December to 26 January at two latitude bands, 0-20°N (left column) and 20-40°N (right column). The same color scales are used for both zonal and meridional winds. Red/blue shadings (positive/negative values) represent eastward/westward winds. The vertical black dashed lines mark the onset of the warming (1 January 2021), where the warming onset is also marked in non-SSW winter plots for comparison. Gray shading designates data gaps.

GOLD Daytime Mean Neutral Temperatures

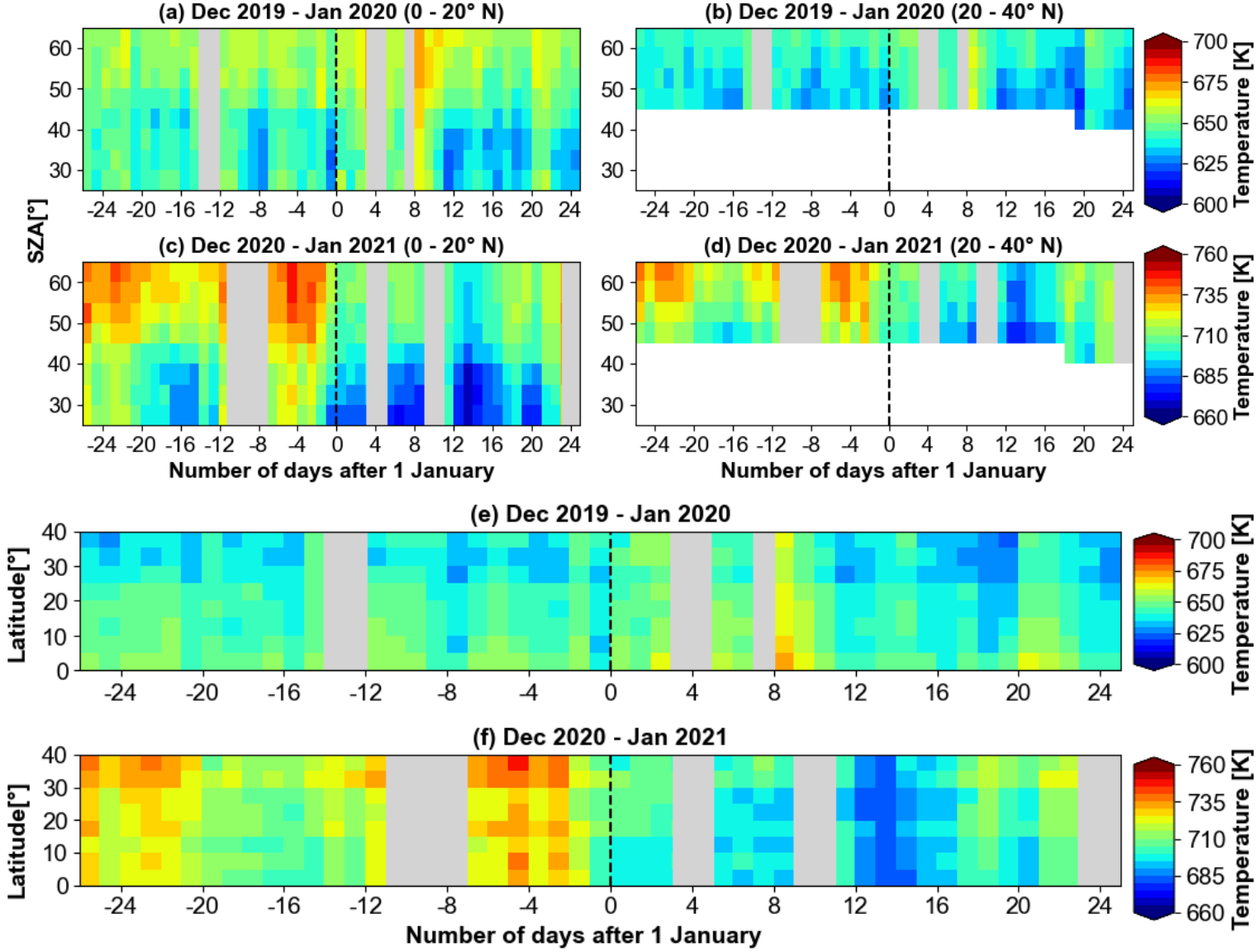


Figure 3. Contour plots of daytime neutral temperatures in K during the non-SSW winter (December 2019-January 2020, first and third rows) and SSW winter (December 2020-January 2021, second and fourth rows) plotted from 6 December to 26 January. Panels a,b,c,d are plotted with respect to the solar zenith angle (SZA) for two latitude bands, 0-20° N (left column) and 20-40° N (right column). Panels e,f are presented as a function of latitude. The light grey shading represents the removed days with A_p index greater than 7. The white shading represents missing data.

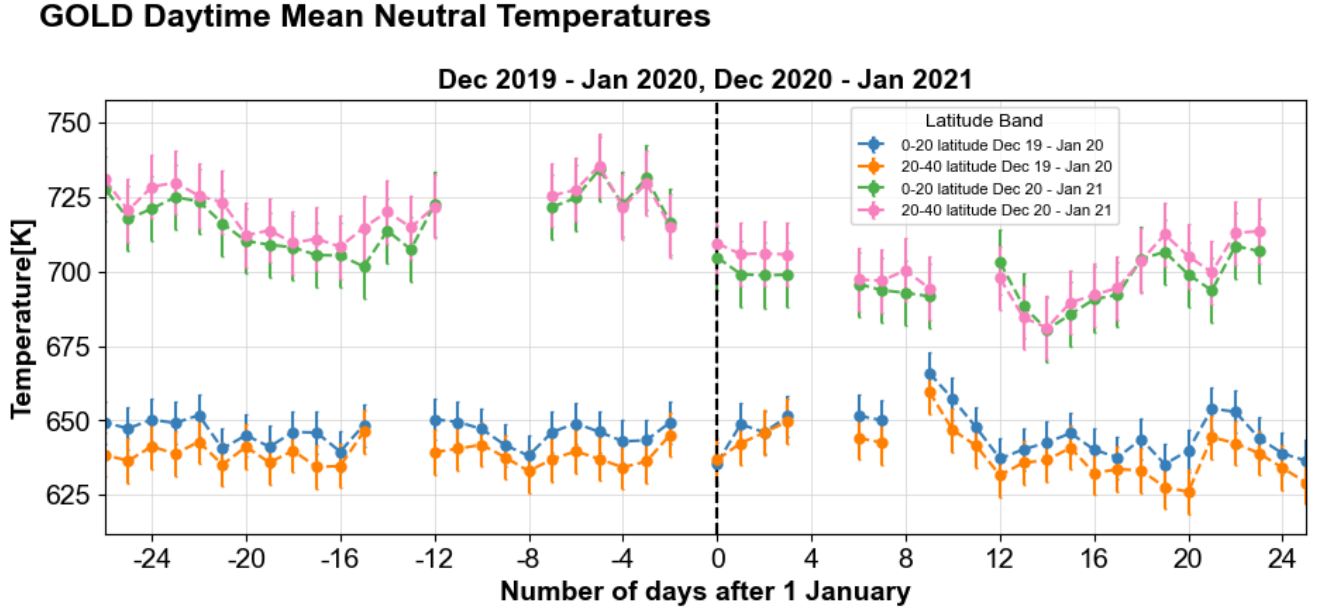


Figure 4. Variation of neutral temperature at different latitude bands. Both SSW and non-SSW winters' temperature average over the respective latitude bands – blue/orange colors (0-20°N/20-40°N) represent the non-SSW winter, and green/pink colors (0-20°N/20-40°N) represent the SSW winter. The vertical black dashed lines mark the onset of the warming (1 January 2021). Warming onset is also marked in non-SSW winter for comparison. Error bars are $\pm\sigma$ of regression residuals.